MEASUREMENT OF HIGH TEMPERATURE POWDER FLOW PROPERTIES TO ESTIMATE INTERPARTICLE FORCES IN HIGH TEMPERATURE FLUIDIZATION

R. Chirone[1], D. Barletta[2], P. Lettieri[1], M. Poletto[2]
1. Department of Chemical Engineering, University College London - London WC1E 7JE - UK
2. Department of Industrial Engineering, University of Salerno - Via Giovanni Paolo II, 132 – 84084 Fisciano (SA) - Italy

Abstract – The High Temperature Annular Shear Cell was used was used to characterise the flow properties of five ceramic powder samples with different particle size distributions at ambient temperature and at 500°C. A significant increase of powder cohesion was observed with increasing temperature. A model combining a continuum approach and a particle–particle interaction description was used to correlate the powder tensile strength with the interparticle forces. The dependence of the tensile strength on powder consolidation and temperature is correctly described by the model.

1. INTRODUCTION

Cohesive flow properties of powders play a key role in several industrial process units, such as fluidized bed reactors, granulators and dryers. Several of these units require high temperature operations, which, in turn, may change powder cohesion with respect to that at ambient temperature. Previous studies on the effect of temperature on fluidization, by means of, bed expansion measurements [1, 2] and bed collapse tests [3-7], showed a change of fluidization behaviour with temperature which cannot be fully explained by taking into account only fluid dynamic forces. These authors provided an interpretation based on the hypothesis that temperature could increase the interparticle forces and their relative weight with respect to body forces. Powder cohesion, in fact, is related to the intensity of interparticle forces such as van der Waals, capillary and electrostatic forces. These forces, in turn, can be affected by temperature as a result of changes of particle hardness, liquid bridges formation or variations of the particle dielectric properties. Direct measurement of interparticle forces as a function of temperature is difficult to perform and is affected by a significant uncertainty [8]. Alternatively, it is possible to measure bulk properties such as the powder cohesion as a function of temperature and to correlate the cohesion change with interparticle forces variations. Few instruments have been developed to measure powder flow properties at high temperature [9, 10]. The High Temperature Annular Shear Cell (HTSC) developed at the University of Salerno is suitable to measure powder yield loci up to 500°C [11].

In this work the HT-ASC was used to characterize the flow properties of five ceramic powder samples with different particle size distributions between ambient temperature and 500°C. Moreover, a model based on the multiscale approach proposed by Rumpf [12] and Molerus [13] was used to predict the effect of temperature on the tensile strength of powder samples.

2. EXPERIMENTAL

2.1 Apparatus and procedure

The High Temperature-Annular Shear Cell (HT-ASC) was used to perform measurements of the powder yield loci at ambient and at 500°C [8]. The annular shear cell has in internal volume of 95cm^3 (60mm inner diameter, 120mm outer diameter, 10mm height) and operates on the same workbench of the original Schulze Ring Shear Tester. The powder sample in the cell is heated by electric heaters placed in the bottom ring and in the lid. Fig. 1 shows a schematic and a picture of the apparatus. Further details are reported by Tomasetta et al. [8].

The experimental procedure was the following. After filling the bottom ring of the cell and positioning it on the desk of the Ring Shear Tester, thermocouples were set and the lid and the weights for consolidation were placed according to the standard procedure. In order to achieve the desired operating temperature, before starting the shear test, heaters were activated and some time was waited to let the temperature reach the desired steady state value. The remaining part of the experimental procedure, used to evaluate the yield loci of the material at the set temperature with the HT-ASC, mainly followed the standard procedure for shear tests with the Schulze Ring Shear Tester [14]. The shear experiments were carried out with the same specimen of powder to measure four different yield loci and in turn to obtain a flow function with four points. In particular, the tests were carried for a major principal stress, σ_1, in the range 1000-1700 Pa. Such low normal stress values were adopted in order to approach a consolidation state relevant to fluidised powders. In fact, fluidization experiments will be performed in future work of the present project. Four shear points were used to derive each yield locus. Each shear experiment was repeated four times in order to increase the statistical significance of the results in terms of yield loci. All the five powder samples were tested at room temperature and high temperature (500°C).
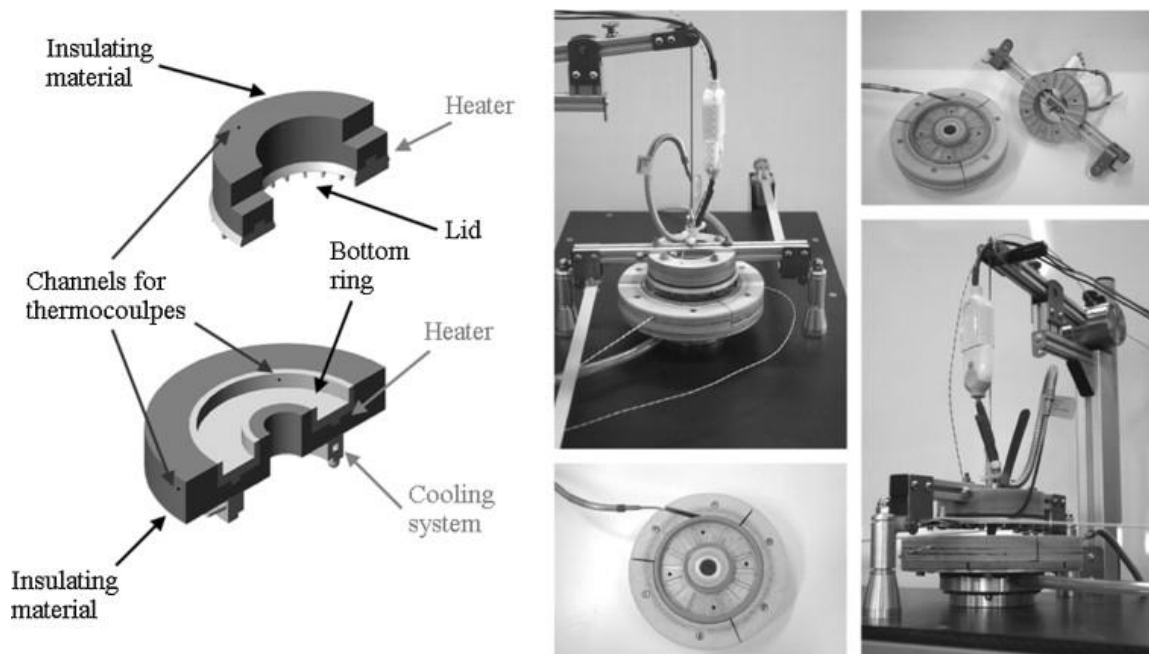
Fig. 1 *Schematic of the High Temperature-Annular Shear Cell (HT-ASC).*

2.2 Materials

The experimental activity have been carried out on five powder samples provided by a private company with different particle size range. In particular, the five cuts were obtained by sieves with nominal mesh size of 20, 38, 63 and 88μm. Corresponding particle size distributions by volume were measured by means of a laser scattering particle size analyser Mastersizer 2000 (Malvern Instruments). Obtained characteristic sizes are reported in Table 1, where d_{32} is the Sauter mean size, d_{43} is the volume weighted mean size, d_{10}, d_{50} and d_{90} are the 10th, the 50th and the 90th percentile size, respectively.

Analysis of the pictures shows some similar features for all the size cuts analyzed: large quantities of fines adhering on the surface of larger particles, irregularly shaped particles with flat surfaces and sharp edges.

Differential Thermal Analysis (DTA), and Thermal Gravimetric Analysis (TGA) were performed by a SDTQ600 (TA Instruments) in order to assess the occurrence of phase transitions and chemical reactions in the temperature range of interest. In particular, the temperature program adopted for these tests provided a linear temperature increase from 25°C to 900°C at 10°C/min. Fig. 3 reports the heat flow and the sample weight as a function of temperature for the 20-38μm sample. Inspection of the heat flow plot reported in the figure reveals that melting or solid phase transitions do not occur in the temperature range investigated. Moreover, constant weight of the sample allows excluding the occurrence of chemical reactions (e.g. oxidation). The thermal behaviour observed for all the other samples was qualitatively similar.

Table 1 *Mean diameters of the five samples tested.*

Particle size, μm	<20μm	20-38μm	38-63μm	63-88μm	>88μm
d_{32}, μm	6.9	22.5	40.6	51.1	104.2
d_{43}, μm	14.0	37.2	62.6	89.1	227.4
d_{10}, μm	3.4	17.7	37.7	55.3	90.3
d_{50}, μm	11.8	35.0	61.3	87.3	184.4
d_{90}, μm	28.1	61.3	95.3	129.7	422.9

A Scanning Electron Microscope SEM was used to observe the sample's surface topography. The Fig. 2 reports typical pictures obtained by SEM analysis for three different samples of the powder (<20μm, 38-63μm, >88μm).
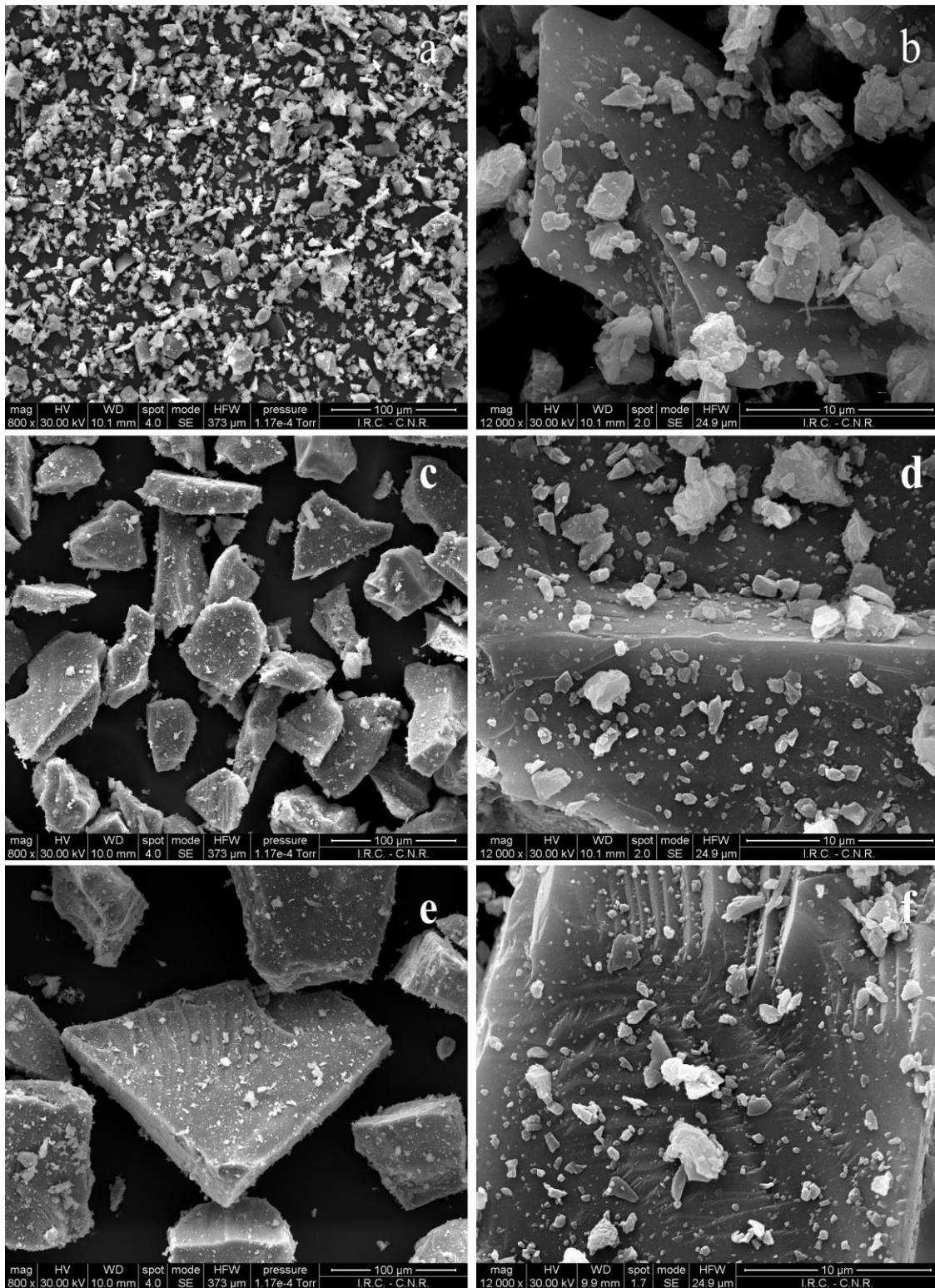
Fig.4 *SEM pictures for the sample smaller than 20μm (a, b), 20-38 μm sample (c, d) and 63-88μm sample (e, f).*
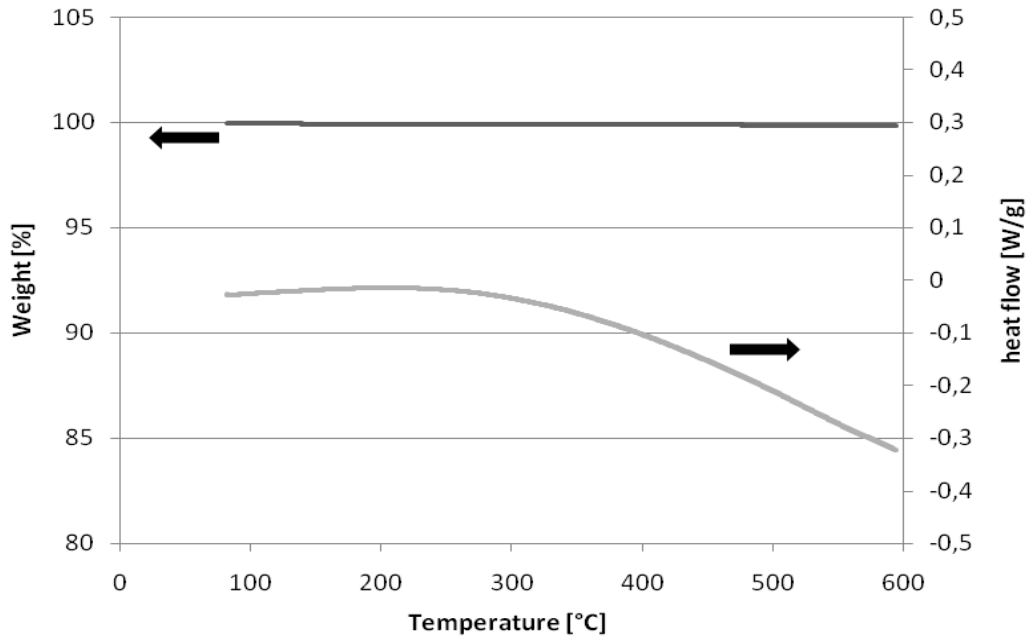
Fig.3 *Heat flow and weight vs temperature obtained by DTA and TGA.*

3. MODEL

Powder flow properties were correlated to interparticle interactions at ambient and high temperature by means of the microscale approaches by Rumpf [12] and by Molerus [13]. The model equations can account alternatively for elastic or plastic deformation of interparticle contact points . In this work, the hypothesis of plastic deformation was assumed according to the results obtained by Tomasetta [15]. This study, in fact, indicated that the assumption of plastic deformation provides the correct order of magnitude values of tensile strength and its dependence on consolidation.

Main assumptions of the model are:
1. Particles are organized in a randomly packed assembly.
2. Particles are spherical and monodisperse.
3. The contact areas between particles are small enough in comparison with the particle surface and therefore contact areas can be assumed as contact points.
4. The contact points are distributed over the particle spherical surface with equal probability.
5. The packing structure is isotropic.
6. The transmission of an isostatic state of compressive stress with three equal principal stresses is assumed.
7. coordination number (i.e., the mean number of contacts of a particle with the adjacent neighbours), k, and assembly porosity, ε, follow the correlation $k\varepsilon \approx 3.1 \approx \pi$ [16, 17].
8. The particle Sauter mean diameter, d_{sv}, is used as the representative particle size.
9. Van der Waals' forces F_{vdW} are the only interparticle forces assumed following the results of the particle thermal analysis.

Starting from these hypotheses, Rumpf (1970) and Molerus (1975) derived the following equation relating the tensile strength, σ_t, with a mean isotropic contact force, F_{vdW}:

$$\sigma_t = \frac{F_{vdW}}{d_{sv}^2} \frac{(1-\varepsilon)}{\varepsilon}$$

(1)

According to equation (1), the tensile strength σ_t of a bulk solid sample is the tensile stress corresponding to the contact separation force equal to the attractive interparticle force at the contact point F_{vdW}.

Equation (1) was used to relate the tensile strength extrapolated from the powder yield locus to the binary interparticle forces. Assuming a plastic irreversible deformation at contact points, Molerus (1975) developed an equation for the adhesion van der Waals force at consolidated contacts:

$$F_{vdW} = \frac{Ar}{12z_0^2} \frac{1+\left(2F_N/\pi p_f r z_0\right)}{1-\left(A/6\pi p_f z_0^3\right)}$$

(2)

Where A is the Hamaker constant, r is the mean curvature radius at contact points (which is not necessarily related to the particle size because of the local curvature or asperities of the particle surface), and z_0 is the separation distance that is usually taken as $z_0 = 0.4$ nm in air [17]. F_N is the compressive force transmitted at the contact during consolidation and p_f is the plastic compressive yield strength of the particle material at the contact point. The combination of equations (1) and (2) provides with an estimate of the tensile strength, given the parameters A, r and z_0. According to equation (2), the magnitude of the van der Waals interparticle force is affected by a factor accounting for the flattening of the contact point, which is a function of the local normal force F_N. The latter is indirectly related to the external consolidation load at the bulk level. Therefore, model equations (1) and (2) can be used to relate the powder tensile strength to powder consolidation. These equations account for powder porosity changes and for changes in the intensity of the binary interparticle interactions.

To calculate the effect of consolidation on the intensity of the binary interaction, the normal contact force F_N that occurs during consolidation must be estimated. Assuming a consolidation stress σ_c, it follows from equation (1) that

$$F_N = \frac{\sigma_c d_{SV}^2 \varepsilon}{\left(1-\varepsilon\right)}$$

(3)

The assumption of uniform distribution of powder consolidation at contact points could be criticised by arguing that not all of the contact points are equally loaded. According to Tomasetta [9] a non-uniform distribution of consolidation forces at contact points F_N does not introduce variations in the estimates of the tensile strength σ_t with the above-proposed procedure.

4. RESULTS AND DISCUSSION

4.1 Experimental results

The flow functions of the five powder samples at ambient temperature are reported in Fig. 4. Inspection of the figure confirms the expected dependence of flowability on the particle size distribution [7]. In particular, according to the Jenike classification for flowability, the finest sample (<20 μm) belongs to the very cohesive class; the 20-38 μm sample belongs to the easy flowing class; the flow functions of the 38-63 μm and the 63-88 μm samples lay on the border between easy flowing and free flowing classes; the coarsest sample (>88 μm) belongs to the free flowing class.
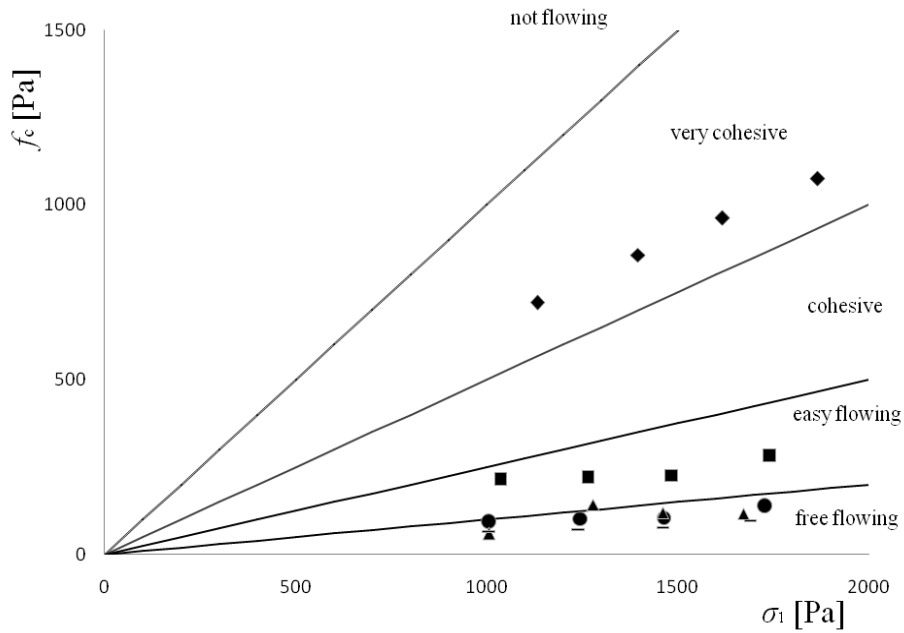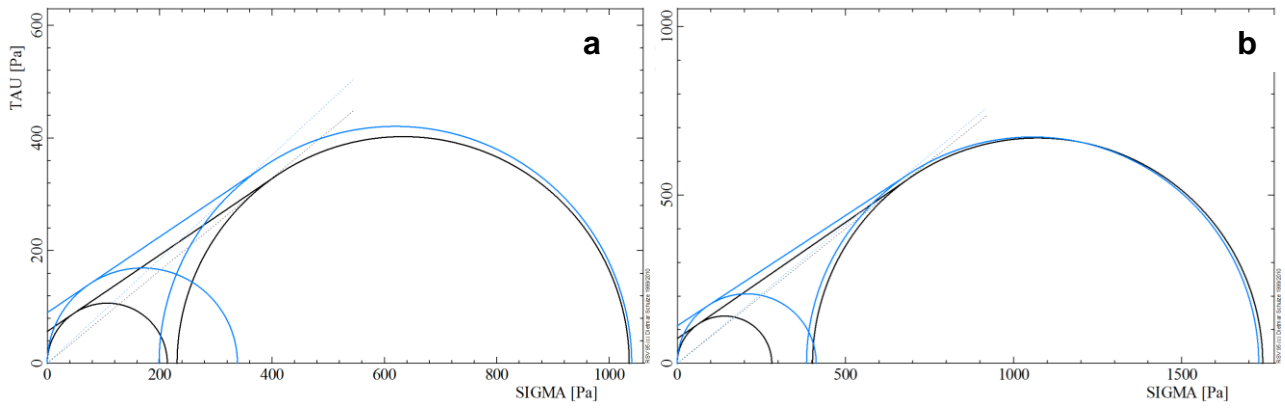
Fig.4 *Flow functions measured with the HT-ASC at 20°C: ◆, sample smaller than 20 μm; ■, 20-38 μm sample; ▲, 38-63 μm sample; ●, 63-88 μm sample, -, sample larger than 88 μm.*

With concern to the effect of temperature on powder flowability, Fig. 5 reports the yield loci of the 20-38 μm sample tested at 25 °C and at 500 °C for $\sigma_1 \approx 1000$ Pa (Fig. 5a) and $\sigma_1 \approx 1700$ Pa (Fig. 5b), as an example of the results obtained for all the samples. The yield loci obtained for the 20-38 μm indicate that cohesion, C, significantly increases with consolidation and temperature (Fig. 5). Differently, the static angle of internal friction, φ, is independent of the consolidation and of the temperature. As a result, the increase of the unconfined yield strength, f_c, with consolidation and temperature is mainly due to the cohesion increase.

Table 2 reports the flow properties (namely, cohesion C, angle of internal friction φ, unconfined yield strength f_c and flow factor, ff) obtained for all the five samples at the lowest and the highest consolidation level as a function of temperature. Fig. 6 reports the flow functions for all the samples at ambient and high temperature.

Inspection of Table 3 and of Fig. 6a reveals that for the finest sample (<20 μm) the yield loci at ambient and high temperature are practically overlapped. Thus, the temperature increase has a negligible effect on cohesion and the powder flow behaviour is very cohesive at both ambient and high temperature. All the other four powder cuts exhibit a significant increase of cohesion with increasing temperature, while the angle of internal friction remains substantially constant (about 34°). For the 20-38 μm sample a 35% increase of cohesion was observed at 500°C. This results in an upward shift of the flow function from the easy flowing class to the cohesive class (Fig. 6b). For the 38-63 μm sample a 40% increase of cohesion was observed at 500°C. This results in an upward shift of the flow function from the free flowing class to the easy flowing (Fig. 6c). A 35% and 45% increase of cohesion was observed at 500°C for the 63-88 μm sample and the coarsest sample (>88 μm), respectively. This results in an upward shift of the flow function of both samples from the free flowing class to the easy flowing (Fig. 6d-e).

Fig.5 *Yield loci for the 20-38 µm sample measured with HT-ASC at 20°C (black line) and 500°C (blue line): a) σ₁ ≈ 1000 Pa ; b) σ₁ ≈ 1700 Pa.*
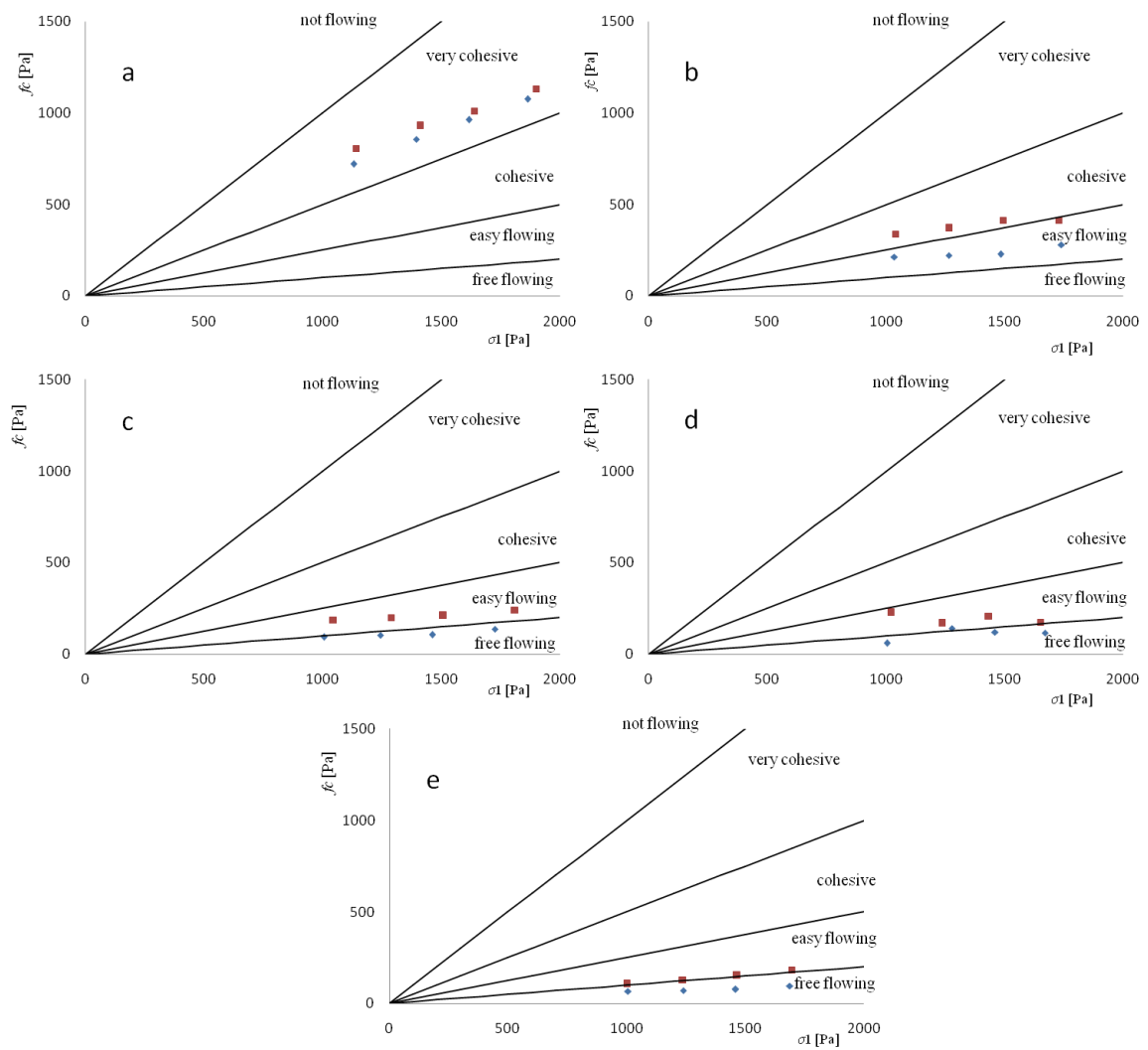
Fig.6 *Flow functions measured with HT-ASC at 20°C (blue diamond) and 500°C (red square): a). sample smaller than 20 µm; b) 20-38 µm sample; c) 38-63 µm sample; d) 63-88 µm sample; e) sample larger than 88 µm.*

Table 2 *Results of the shear tests performed with HT-ASC.*

Sample	$T(°C)$	σ_1 (Pa)	C (Pa)	φ (°)	f_c (Pa)	$f\!f$ (-)
<20 µm	20	1132	191	34	720	1.57
	500	1141	211	34.8	807	1.41
	20	1866	283	34.4	1075	1.74
	500	1900	288	36.1	1133	1.68
20-38 µm	20	1036	57	34.2	214	4.85
	500	1040	90	33.9	338	3.07
	20	1741	74	34.6	281	6.19
	500	1729	112	33.2	413	4.18
38-63 µm	20	1007	25	33.2	93	10.78
	500	1047	47	34.1	186	5.63
	20	1728	37	33.8	138	12.48
	500	1812	61	36.2	240	7.56
63-88 µm	20	1279	38	34.4	142	9.02
	500	1238	45	33.3	168	7.35
	20	1672	31	34.1	117	14.34
	500	1653	47	33.6	175	9.43
>88 µm	20	1006	17	35.7	66	15.34
	500	1001	27	36.1	105	9.51
	20	1689	25	34.8	96	17.68
	500	1697	47	35.8	182	9.30

4.2 Model results

The model described in section 3 was applied to the experimental materials. A unique value of the Hamaker constant was assumed for all samples and temperatures [18]. Instead, accounting for thermal expansion and thermal effects on mechanical properties of the particle material, different values of particle density ρ_p and compressive strength p_f [19] were adopted at 25°C and 500°C, as reported in Table 3. Furthermore, sample porosity ε was derived from experimental values of bulk density, ρ_b, measured during shear tests and from the particle density.

Table 3 *Particle properties used in the model at ambient and high temperature.*

T [°C]	ρ_p [kg m^{-3}]	A [10^{-20} J]	p_f [GPa]
25	2330	20	12
500	2320	20	4.5

Experimental values of cohesion C and angle of internal friction φ were used to estimate the powder tensile strength by the following equation:

$$\sigma_t = \frac{C}{\tan\varphi}$$

(4)

Substituting this σ_t value in Eq. (1) and the experimental σ_c value in Eq. (3), combining Eqs. (1) to (3), the mean curvature radius r was evaluated for all samples and experimental conditions. Results in terms of interparticle forces, mean curvature radius and other bulk properties are reported in Table 4. Inspection of this table indicates that the mean curvature radius value generally varies with the particle size of the sample and with temperature.

Table 4 *Mean results of the mathematical model.*

sample	T	σ_c	ρ_b	ε	σ_t	F_{VdW}	Fn	r
	°C	Pa	kg m^{-3}	-	Pa	nN	nN	μm
<20 μm	25	541	682.1	0.71	270.6	311	622	0.29
	25	666	704.6	0.70	346.2	380	731	0.35
	25	790	720.8	0.69	354.4	377	840	0.35
	25	915	737.0	0.68	413.3	425	942	0.39
<20 μm	500	538	604.7	0.74	349.4	472	727	0.41
	500	633	623.3	0.73	305.4	396	820	0.34
	500	787	638.0	0.73	310.2	389	988	0.33
	500	912	652.7	0.72	335.3	408	1109	0.34
20-38 μm	25	547	983.3	0.58	84.2	584	3793	0.50
	25	672	999.4	0.57	85.3	575	4530	0.48
	25	796	1014.3	0.56	83.6	549	5227	0.45
	25	921	1028.1	0.56	107.3	688	5904	0.57
20-38 μm	500	544	899.3	0.61	133.9	1071	4351	0.84
	500	669	918.9	0.60	149.6	1155	5165	0.88
	500	793	916.6	0.60	176.0	1365	6148	1.04
	500	917	925.8	0.60	171.2	1305	6992	0.96
38-63 μm	25	554	1027.0	0.56	38.2	799	11586	0.60
	25	679	1044.0	0.55	42.6	865	13787	0.64
	25	803	1056.0	0.55	41.5	826	15969	0.57
	25	928	1067.0	0.54	55.3	1078	18107	0.78
38-63 μm	500	552	970.0	0.58	62.8	1441	12664	0.88
	500	676	982.0	0.58	73.4	1650	15183	0.99
	500	800	980.0	0.58	71.9	1620	18032	0.86
	500	924	984.0	0.58	83.3	1865	20680	0.99
63-88 μm	25	553	1128.2	0.52	27.7	772	15383	0.53
	25	677	1119.0	0.52	45.5	1287	19133	0.96
	25	801	1116.7	0.52	44.4	1261	22727	0.89
	25	801	1353.6	0.42	45.8	862	15089	0.62
63-88 μm	500	553	1109.8	0.52	70.5	2007	15749	1.30
	500	675	1062.6	0.54	68.5	2117	20858	1.22
	500	800	1069.5	0.54	64.5	1969	24426	0.96
	500	927	1162.7	0.50	70.7	1839	24097	0.85
>88 μm	25	559	1243.0	0.47	23.7	2246	53077	1.42
	25	685	1283.0	0.45	25.2	2236	60694	1.31
	25	808	1279.0	0.45	27.8	2483	72091	1.39
	25	612	1269.0	0.46	28.8	2612	55557	1.74
>88 μm	500	560	1159.0	0.50	37.0	4027	60911	1.57
	500	684	1167.0	0.50	46.1	4945	73380	1.98
	500	809	1186.0	0.49	54.7	5677	83992	2.28
	500	932	1181.0	0.49	65.2	6824	97600	2.86

Assuming a mean curvature radius constant with temperature, the model can predict the effect of temperature on the tensile strength. In particular, $r = 0.35$ μm was assumed for the finest sample (<20 μm), while $r = 1.06$ μm was used for all the other samples. The tensile strength values obtained by the application of the model with these further assumptions were compared with the experimental tensile strength values in the parity plot reported in Fig. 7. The comparison shows a very good matching between model values and experimental values. This result allows concluding that assuming a reasonable value of the mean curvature radius at the contact points, the model is able to predict the correct order of magnitude of the tensile strength.
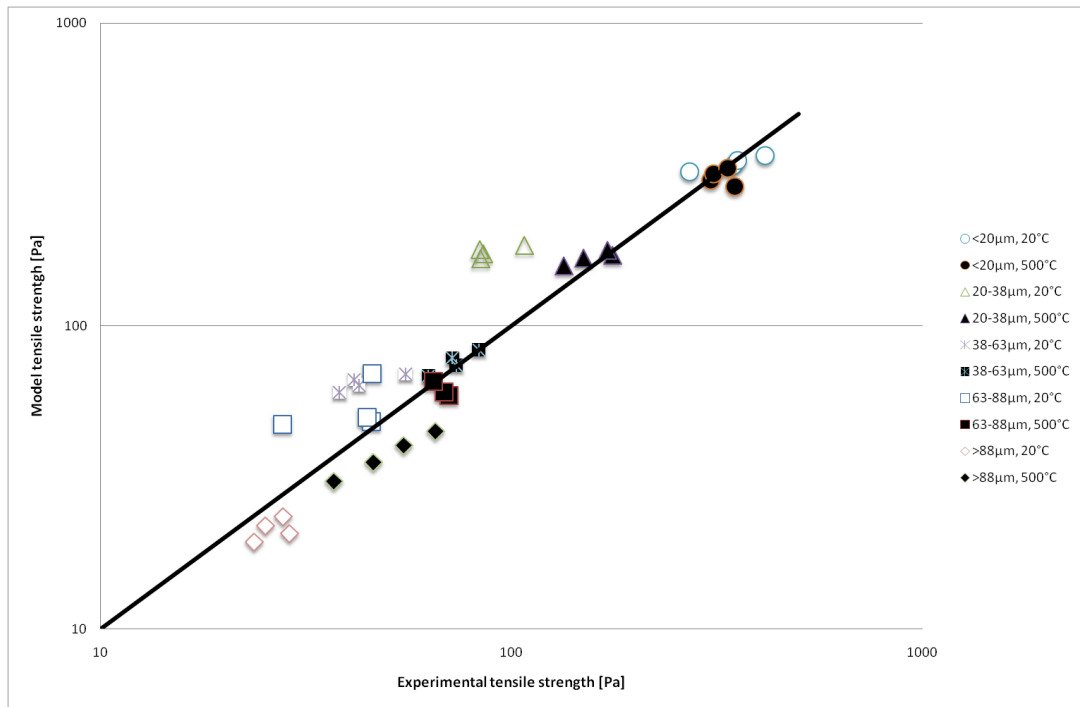
Fig.7 *Experimental tensile strength vs tensile strength model predictions.*

5. CONCLUSIONS

Shear experiments highlighted a significant increase of powder cohesion at 500°C for different cuts of the same powder with a particle size larger than 20 μm. This resulted in a lower flowability of the samples. Thermal analysis on the powder samples revealed that the temperature effect on powder flow properties is only due to van der Waals forces.

A model combining the continuum approach and the particle–particle interaction description was used to correlate the powder tensile strength with the interparticle forces. The model with the assumption of plastic deformation at contact points is able to predict the correct order of magnitude of the tensile strength provided a reasonable value of the mean curvature radius at the contact points. Furthermore, the dependence of the tensile strength on powder consolidation and temperature is correctly described by the model.

NOMENCLATURE

A	parameter in equation (2)	N
A	Hamaker constant	N m
C	powder cohesion	Pa
d	particle diameter	m
d_{10}	10th percentile particle diameter	m
d_{50}	50th percentile particle diameter	m
d_{90}	90th percentile particle diameter	m
d_{sv}	particle Sauter mean diameter	m
F_c	mean isotropic contact force	N
f_c	unconfined yield strength	Pa
ff	flow factor	-

F_N	mean isotropic consolidation force at the particle contact	N
F_{vdW}	mean isotropic van der Waals force at the particle contact	N
k	coordination number	-
p_f	particle material compressive strength	Pa
r	mean curvature radius at contact points	m
T	temperature	°C
z_0	interparticle separation distance	m

Greek symbols

ε	porosity of the bulk solid	-
φ	angle of internal friction	deg
ρ_b	bulk density	kg m^{-3}
ρ_p	particle density	kg m^{-3}
σ	normal stress	Pa
σ_1	major principal stress	Pa
σ_c	normal stress at consolidation	Pa
σ_f	compressive yield strength	Pa
σ	tensile strength of the bulk solid	Pa
τ	shear stress	Pa

REFERENCES

[1] H.Y. Xie, D. Geldart, Fluidization of FCC powders in the bubble-free regime: effect of types of gases and temperature, Powder Technol. 82 (1995) 269–277.

[2] P. Lettieri, D. Newton, J.G. Yates, Homogeneous bed expansion of FCC catalysts, influence of temperature on the parameters of the Richardson–Zaki equation, Powder Technol. 123 (2002) 221–231.

[3] B. Formisani, R. Girimonte, L. Mancuso, Analysis of the fluidization process of particle beds at high temperature, Chem. Eng. Sci. 53 (1998) 951–961.

[4] B. Formisani, R. Girimonte, G. Pataro, The influence of operating temperature on the dense phase properties of bubbling fluidized beds of solids, Powder Technol. 125 (2002) 28–38.

[5] P. Lettieri, J.G. Yates, D. Newton, The influence of interparticle forces on the fluidization behaviour of some industrial materials at high temperature, Powder Technol. 110 (2000) 117–127.

[6] P. Lettieri, D. Newton, J.G. Yates, High temperature effects on the dense phase properties of gas fluidized beds, Powder Technol. 120 (2001) 34–40.

[7] G. Bruni, P. Lettieri, D. Newton, J. Yates, The influence of fines size distribution on the behaviour of gas fluidized beds at high temperature, Powder Technol. 163 (2006) 88–97.

[8] P. Pagliai, S.J.R. Simons, D. Rhodes, A novel experimental study of temperature enhanced cohesive interparticle forces, Powder Technol., 174 (2007), 71–74.

[9] H. Kamiya, A. Kimura, T. Yokoyama, M. Naito, G. Jimbo, Development of a split-type tensile-strength tester and analysis of mechanism of increase of adhesion behavior of inorganic fine powder bed at high-temperature conditions, Powder Technol. 127 (2002), 239-245.

[10] M. Ripp, S. Ripperger, Influence of temperature on the flow properties of bulk solids, Chem. Eng. Sci., 65 (2010), 4007–4013.

[11] I. Tomasetta, D. Barletta, M. Poletto, The high temperature annular shear cell: A modified ring shear tester to measure the flow properties of powders at high temperature, Advanced Powder Technol., 24 (2013), 609‑617.

[12] H. Rumpf, Zur Theorie der Zugfestigkeit von Agglomeraten bei Kraftübertragung an Kontaktpunkten, Chemie Ingenieur Technik, 42 (8) (1970), 538-540.

[13] O. Molerus, Theory of yield of cohesive powders, Powder Technology, 12 (1975), 259-275.

[14] ASTM D6773-02 Standard Shear Test Method for Bulk Solids Using the Schulze Ring Shear Tester.

[15] I. Tomasetta, D. Barletta, M. Poletto, Correlation of powder flow properties to interparticle interactions at ambient and high temperatures, Particuology, vol.12 (2014), 90-99.

[16] W.O. Smith, P.D. Foote, P.F. Busang Packing of homogeneous spheres Physical Review, 34 (1929), 1271-1274.

[17] H. Krupp, Particle adhesion theory and experiment, Advances in Colloid and Interface Science, 1 (1967), 211–239.

[18] Israelachvili, J. N. Intermolecular and surface forces: revised third edition. Academic press. (2011).

[19] V. Domnich, Y. Aratyn, W.M. Kriven, Temperature dependence of silicon hardness: experimental evidence of phase transformations, Rev. Adv. Mater. Sci., 17 (2008), 33-41.